



ELSEVIER

Coastal Engineering 46 (2002) 233–247

**Coastal
Engineering**
An International Journal for Coastal,
Harbour and Offshore Engineers

www.elsevier.com/locate/coastaleng

Field experiment on secondary wave generation on a barred beach and the consequent evolution of energy dissipation on the beach face

N. Sénéchal*, P. Bonneton, H. Dupuis

Department of Geology and Oceanography, UMR CNRS 5805, University of Bordeaux I, 33405 Talence, France

Received 12 June 2001; received in revised form 28 March 2002; accepted 16 July 2002

Abstract

A field experiment, conducted on a sandy, barred beach situated on the southern part of the French Atlantic coastline, allowed us to investigate the formation of secondary waves when a moderate (significant wave height of about 0.8 m in 3.7-m water depth), long (11–14 s) narrowband swell propagated over an intertidal ridge and runnel system, in both breaking and nonbreaking conditions. Field evidence using higher spectral analysis is given for the sum interactions between pairs of waves at the primary spectral peak and the consequent energy transfer to nearly harmonic wave components. Although wave breaking appears to weaken the strength of nonlinear couplings, the generation of high-frequency energy is hardly affected by wave breaking. The phenomenon of harmonic decoupling, which takes place behind the bar, cannot be completely ascribed to the increase in water depth and the so-called deshoaling effect. Indeed, the variation in the values of the maximum bicoherence was very moderate when no breaking occurred. Finally, the doubling in the number of wave crests and the consequent decrease in the significant wave period delay the energy dissipation on the beach face.

© 2002 Elsevier Science B.V. All rights reserved.

Keywords: Surf zone; Secondary wave generation; Sandy barred beach; Field experiment; Bicoherence spectrum

1. Introduction

As ocean surface waves shoal from deep to shallow water, amplitudes increase, wavelengths decrease, and propagation directions refract toward normal incidence to the beach. However, in addition to these linear propagation effects, it has been increasingly

recognized that nonlinearity manifests itself in various gravity wave phenomena. In particular, triad interactions in shallow water are important for a number of physical processes (bound, long-wave generation, secondary wave generation, wave profile deformation, etc.) and explain significant transfers of energy to wave components with both higher and lower frequencies (Freilich and Guza, 1984; Elgar and Guza, 1985; Masselink, 1998; Ruessink, 1998).

Nonlinear interactions between two primary wave components with frequencies and (vector) wave numbers (ω_1, k_1) and (ω_2, k_2) excite secondary waves

* Corresponding author. Tel.: +33-5-56-84-83-81; fax: +33-5-56-84-08-48.

E-mail address: n.senechal@geocean.u-bordeaux.fr (N. Sénéchal).

with the sum ($\omega_1 + \omega_2 = \omega_3$, $k_1 + k_2 = k_3$) and difference ($\omega_1 - \omega_2 = \omega_3$, $k_1 - k_2 = k_3$) of frequency and wave number. The nonlinearly excited secondary wave components are phase-locked to the statistically independent primary wave components incident from deep water and thus cause deviations from Gaussian statistics of surface elevation (e.g., steep and asymmetric wave profiles).

For sufficiently long and high incident waves, submerged bars or shelf with a finite width can induce the decomposition phenomenon of a nonlinear wave train. Generation of higher harmonics in wave propagating over submerged obstacles has long been known. Johnson et al. (1951) noted that over natural reefs, the energy was transmitted as a multiple crest system. Since then, this decomposition phenomenon has been observed both in field measurements (Elgar et al., 1997; Masselink, 1998), in physical model experiments (Rey et al., 1992; Driscoll et al., 1992; Beji and Battjes, 1993; Brossard and Chagdali, 2001), and in numerical wave tanks (Ohyama and Nadaoka, 1994; Grilli and Horrilli, 1999).

Beji and Battjes (1993) showed that the generation of high-frequency energy and its transfer among nearly harmonic wave components due to the nonlinear interactions taking place in the course of waves' passage over the bar is hardly affected by wave breaking,

which acts merely as a secondary effect, by simply rescaling the wave spectrum through overall energy dissipation. The phenomenon of harmonic decoupling, which takes place as the waves propagate in the deepening water (downslope) resulting from the deshoaling, plays a major role in the wave decomposition and in redistributing the total energy among the primary wave and harmonics and thus determining the final spectral shape.

Ohyama and Nadaoka (1994) showed that a large amount of energy in bound harmonics over the shelf is abruptly transmitted into free, higher harmonics in the tailing side of the shelf. They also showed that in the case of large incident waves, significant decomposition takes place even when the shelf is deeply submerged.

Despite the significance of secondary waves in natural surf zones, there is a paucity of field investigations on this topic. The subject matter of this study is to extend the precedent field experiment analysis in the case of a moderate, long, and narrowband incoming swell. It is concerned with the generation of harmonics induced by long waves propagating over a submerged bar and their decomposition into shorter components. It aims at going into the present works thoroughly, by use of higher spectral analysis (bispectrum) applied to data collected during a field experiment conducted on the Truc Vert Beach (see thereafter), which presented a

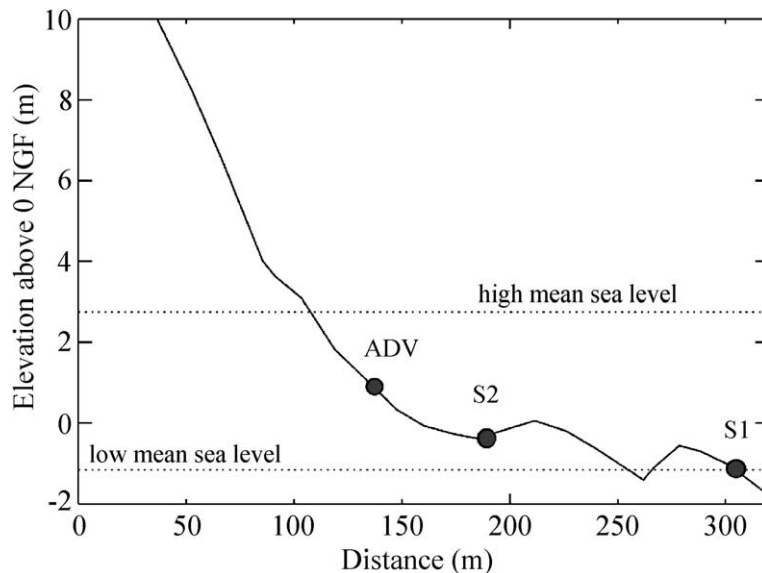


Fig. 1. Beach profile of Truc Vert Beach and sensor deployment.

double ridge and runnel system in the lower part of the intertidal zone (Fig. 1), and then to analyze the impact on wave energy dissipation on the beach face. Preliminary definitions and properties of the bispectrum are reviewed in Section 2, and the field experiment is described in Section 3. Generation of harmonics for both breaking and nonbreaking waves is discussed in Section 4, where phenomena undetectable with one-dimensional spectral analysis are presented. Implications for wave energy dissipation in the surf zone are discussed in Section 5.

2. Definitions and properties of the bispectrum

The bispectrum was introduced by Hasselman et al. (1963) to examine weak wave nonlinearity in intermediate water depths. Indeed, the energy spectrum (defined as the Fourier transform of the second-order correlation function of the time series) is independent of the phases. If the phases of Fourier components are not random but are statistically correlated, the sea surface is not Gaussian (Hasselman et al., 1963). Departure from Gaussian form cannot be detected by the energy spectrum. Higher-order spectra such as the bispectrum, which is an ensemble average of a product of three spectral components, is shown to be a very useful diagnostic tool in experimental studies of nonlinear wave interactions and can be used to investigate nonlinearity even in shallow water, where wave's nonlinearities can become very strong (Elgar and Guza, 1985; Eldeberky, 1996; Becq, 1998). In particular, it is shown that the bicoherence spectrum (the normalized magnitude of the bispectrum) may be used to discriminate between nonlinearly coupled waves and spontaneously excited waves and to measure the fraction of wave power due to the quadratic wave coupling in a self-excited fluctuation spectrum (Kim and Powers, 1979).

The bispectrum is a complex quantity, formally defined as the Fourier transform of the third-order correlation function of the time series:

$$B(\omega_1, \omega_2) = \left[\frac{1}{2\pi} \right] \int_{-\infty}^{+\infty} \int_{-\infty}^{+\infty} R(\tau_1, \tau_2) \times \exp[-i(\omega_1\tau_1 + \omega_2\tau_2)] d\tau_1 d\tau_2 \quad (1)$$

in which

$$R(\tau_1, \tau_2) = \langle \eta(t)\eta(t + \tau_1)\eta(t + \tau_2) \rangle \quad (2)$$

and η is the sea-surface elevation; τ is a time lag, and $\langle \rangle$ denotes the expected value or average operator.

The digital (discrete) bispectrum, appropriate for discretely sampled data, is (Kim and Powers, 1979):

$$B(k, l) = \langle A_k A_l A_{k+l}^* \rangle \quad (3)$$

where A_ω is complex Fourier amplitude and an asterisk indicates complex conjugation.

Similarly, the power spectrum is defined here as:

$$P(k) = \frac{1}{2} \langle A_k A_k^* \rangle \quad (4)$$

The bispectrum $B(\omega_1, \omega_2)$ vanishes if:

- there is no energy present at frequencies k or l , or $k \pm l$ (i.e., zero Fourier amplitude of any component participating in the triad interactions);
- there is no phase relation (coherence) between the waves forming the triad (i.e., statistically independent free waves).

The bispectrum can be used to identify coupled modes; however, it does not give a quantitative value of the intensity of nonlinear interactions because its value depends on the amplitudes of the three waves involved in the interaction. It is convenient to cast the bispectrum into its normalized magnitude and phase, the so-called bicoherence and biphase given, respectively, by (Kim and Powers, 1979):

$$b_{k,l}^2 = \frac{|B_{k,l}|^2}{\langle |A_k A_l|^2 \rangle \langle |A_{k+l}|^2 \rangle} \quad (5)$$

$$\beta_{k,l} = \arctan \left[\frac{\text{Im}\{B_{k,l}\}}{\text{Re}\{B_{k,l}\}} \right] \quad (6)$$

Clearly, the bicoherence is independent of the wave amplitude unlike the bispectrum. For this bicoherence normalization (Eq. (5)), $0 \leq b^2 \leq 1$. For a three-wave system, Kim and Powers (1979) show that $b^2(k, l)$ represents the fraction of power at frequency $k+l$ due to quadratic coupling of the three modes (k, l , and $k \pm l$). No such simple interpretation for the bicoherence is possible in a broad-band process, where a

particular mode may be simultaneously involved in many interactions (McComas and Briscoe, 1980). Nevertheless, the bicoherence does give an indication of the relative degree of phase coupling between triads of waves, with $b=0$ for random phase relationships and $b=1$ for a maximum amount of coupling.

For a finite-length time series, even a truly Gaussian process will have a nonzero bispectrum. A 95% significance level on zero bicoherence is given by Haubrich (1965) as

$$b_{95\%}^2 \geq 6/dof \quad (7)$$

where dof is the degrees of freedom in the bispectral estimates.

3. Field experiment and data reduction

3.1. The study area

This study is based on data collected during one fieldwork carried out for 2 days in March 2000. This fieldwork is part of a French national research project (Programme National Environments Côtiers) on sandy beach evolution. The data described in this paper were collected at Truc Vert Beach, which is situated on the southern part of the French Atlantic coastline at approximately 10 km north of the Cap Ferret spit at the mouth of the Arcachon lagoon. Truc Vert Beach is typical of the relatively undisturbed coast extending 100 km between the Gironde estuary (90 km to the north) and the Arcachon inlet (10 km to the south). This is a low, sandy coast, almost N–S orientated and bordered by high aeolian foredunes. The sediment consists primarily of a medium-grained quartz sand with a median particle size of around 350 μm (Lorin and Viguié, 1987). Truc Vert Beach is of the intermediate type 2e (following Masselink and Short, 1993) and exhibits a ridge and runnel system in the dissipative, lower intertidal domain and a steeper beach face (Fig. 1). Off the beach, crescentic, long-shore bars are found, as described in Froidefond et al. (1990) and more recently in Lafon et al. (in press).

This coast is exposed to almost continuous, moderate energy swell originating mainly from the north–northwest. Based on wave rider measurements in 26-m water depth, the wave climate is of the oceanic

type, with an average mean period of 6.5 s and a mean significant wave height of 1.4 m (Butel et al., 2002). The meso-macrotidal regime (approximately 4.5-m tidal range at spring tides), with a relatively broad intertidal region (around 200 m), allows instrumentation to be safely deployed and recovered at low tide, while measurements can be obtained at high tide.

3.2. Field experiment

Changes in the beach profile were very small during the 2 days in March 2000, when the observations discussed here were obtained. The beach exhibited a double ridge and runnel system in the lower part of the intertidal zone (Fig. 1). The first bar has a seaward slope around 0.03 and a landward slope around 0.05. At high tide, the bar is in about 3.2-m water depth, and the first trough is in about 4-m water depth. The second bar (located landward from the precedent bar) has a seaward slope around 0.03 and a landward slope around 0.02. At high tide, it is in about 2.5-m depth, and the second trough is in about 3.0-m depth. The beach face in the upper intertidal zone has a slope of about 0.06.

Pressures were measured at three locations in the intertidal zone using one bottom-mounted Acoustic Doppler Velocimeter (ADV Vector) from Nortek and two bottom-mounted Directional Wave Current Meter (S1 and S2) from InterOcean System. The height used in this analysis was set around 0.5 m above the bed for sensors S1 and S2, and around 0.05 m for the ADV pressure sensor.

The outer station (S1) was positioned on the seaward face of the first bar, corresponding to the low water mark. This station, situated in about 3.7-m water depth at high tide, served as the reference gage for the incident waves. Station S2 was deployed in the second trough and served to analyze the bar effect on the wavefield (by comparing with data collected at station S1). Station ADV was located on the plane beach (Fig. 1) and permitted to analyse the wavefield evolution. Data run were continuously acquired at a 2-Hz sample rate for S1 and S2 during all the fieldwork. Concerning the ADV, the signals were continuously sampled at 8 Hz in March 21, 1 h during rising tide conditions and 2 h during falling tide conditions, and at 32 Hz in March 22, 90 min during rising tide conditions and 40 min during falling tide conditions.

The 21st-of-March wave field was dominated by a narrowband swell (peak period around 11 s) from a distant, atmospheric low in the North Atlantic. The significant wave height (defined here as four times the sea-surface standard deviation) in 3.7 m (at high tide) was about 0.75 m. Wave crest spread parallel to the coastline. Currents were very low, even at sensor S2 situated in the trough. Indeed, at this sensor, for the entire selected data period, long-shore currents were always orientated southward with a mean value (about 0.5 m above the sea floor) of about 0.1 m/s; cross-shore currents were always orientated westward with a mean value about 0.07 m/s.

The 22nd-of-March wave field was also dominated by a narrowband swell (peak period around 14 s). The significant wave height in 3.7 m (at high tide) was about 0.90 m. Wave crest spread parallel to the coastline. Concerning the currents, conditions were the same as the previous day.

On the first day, waves at high tide were breaking only on the beach face, whereas for the second day, waves at high tide were generally breaking on the landward bar, predominantly by plunging, but were rapidly (after several meters) transformed into bore-like broken waves; a second breakpoint was present on the beach face. For both days, waves during rising and falling conditions were breaking on the second bar, predominantly by plunging, but were rapidly (on several meters) transformed into bore-like broken waves. The broken waves decomposed then into smaller waves as they propagated across the trough. A secondary breakpoint was present on the beach face.

3.3. Data reduction and methods

Concerning stations S1 and S2 for March 21, only 6 h of data were selected for analysis centered on the high-tide level and for March 22, 6 h of data were also selected corresponding to 4 h before high tide and 2 h after high tide.

All hydrodynamic data were processed similarly. First, pressure measurements were converted to water elevations. Outside the surf zone, a correction factor as proposed in Horikawa and Kubota (1988) was applied to account for the pressure field being nonhydrostatic. This correction generates a high-frequency cutoff, corresponding to the limit of the sensor sensitivity

according to its immersion and the water depth attenuation of the waves. The high-frequency cutoff of $F_{hi}=0.4$ Hz was applied to the whole data set.

In the surf zone, sea-surface elevations were estimated assuming that the pressure field is hydrostatic. Indeed, as shown by Lin and Liu (1998), using a numerical model based on the Reynolds equations, the pressure distribution under the spilling, breaking wave is almost hydrostatic, with a maximum deviation from hydrostatic pressure of only 7%, which occurs under the broken wavefront.

For spectral and bispectral analysis, the selected data were processed by breaking the entire record into consecutive sections of 1200 s each. Power spectral and bispectral estimates were calculated by Fourier transforming overlapping (75%), Hanning-windowed, and detrended 4-min data segments averaged over 20 min. The final resolution of spectral estimates is 0.004 Hz, and the degrees of freedom in the spectra discussed here is 34. Statistical stability of bispectral estimates was gained by averaging bispectral values over 5×5 squares. The final bispectral resolution is 0.02 Hz, and the degrees of freedom in the bispectra discussed here was 170. Thus, the 95% significance level on zero bicoherence (Eq. (7)) is $b=0.2$.

For energy dissipation in the surf zone, because the mean sea level above the sensors was subject to tidal variations, the selected data were processed by breaking the entire record into consecutive sections of 600 s each (periods while tidal variations of the sea-surface elevation are less than 15%).

In the following, two cases will be discussed: the breaking case when waves were breaking between sensors S1 and S2 and another breakpoint was present on the beach face, and the nonbreaking case when only one breakpoint was present on the beach face. A third case corresponding to wave breaking before the ridge and runnel system was also possible, but it will not be investigated because it occurred when S2 and ADV sensors were not continuously immersed.

4. Results

4.1. Time domain records

Figs. 2 and 3 show 120-s synchronized sections of the water-surface elevation data at (a) sensor S1 and

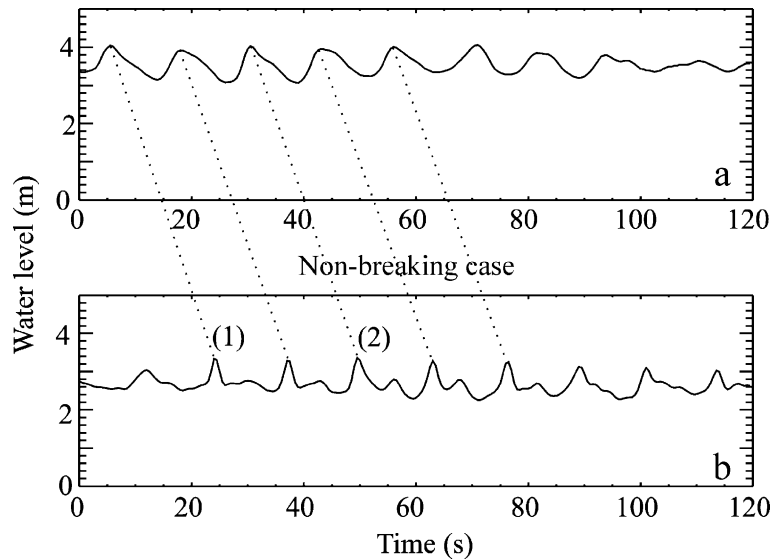


Fig. 2. Segment of detrended water-surface elevation data for sensors (a) S1 and (b) S2 in the nonbreaking case. The dotted lines follow the wave fronts along their propagation toward the beach. (1) Indicates the generation of the so-called dispersive tail waves and (2) indicates its decomposition into a secondary wave.

(b) sensor S2. In the nonbreaking case (Fig. 2), station S1 was located in about 3.6-m water depth and station S2 in about 2.7 m. In the breaking case (Fig. 3), station S1 was located in about 3.2-m water depth and

station S2 in about 2.3-m water depth. It is worth noting that as observed in previous works (Beji and Battjes, 1993; Masselink, 1998), wave breaking (Fig. 3b) does not alter the characteristic waveform drasti-

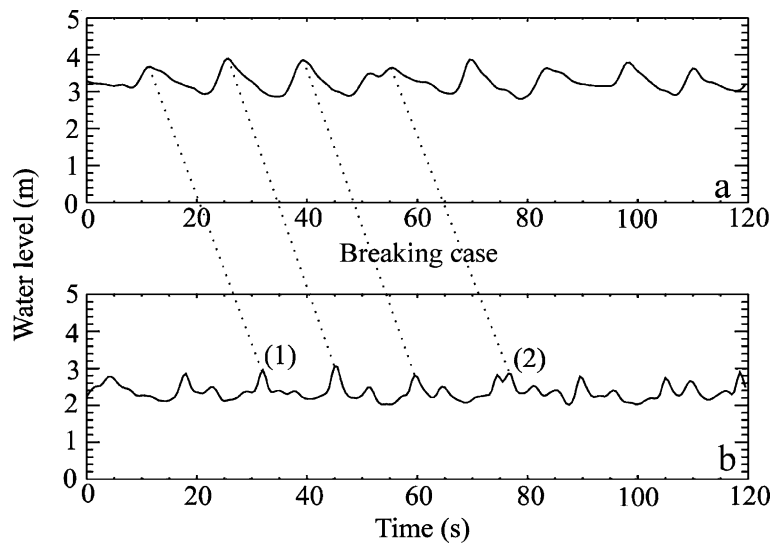


Fig. 3. Segment of detrended water-surface elevation data for sensors (a) S1 and (b) S2 in the breaking case (see legend for the dotted lines and the numbers in Fig. 2).

cally so as to make it incomparable with its unbroken counterpart (Fig. 2b). Indeed, we clearly observe, in both cases, the formation of the so-called dispersive tail waves (i.e., wave 1) and also its decomposition into several, smaller amplitude waves of nearly harmonic frequencies (i.e., wave 2). This is consistent with previous field observations. Elgar et al. (1997) observed a doubling in the number of wave crests when moderately energetic (about 0.8 m significant wave height in 8-m depth) narrowband swell propagated without breaking across an 80-m-wide, nearly flat section of beach, between a small, offshore sand bar and a steep beach face, where the waves finally broke. Masselink (1998) observed that both breaking and nonbreaking waves decomposed into smaller waves as they propagated across the flat section of the bar and passed over the bar edge. According to previous observations, the presence of the second bar does not alter the characteristic waveform drastically so as to make it incomparable with the cases previously observed by other authors (Elgar et al., 1997; Masselink, 1998), where only one bar was present.

4.2. Spectral evolution

The change in partitioning of the wave potential energy is also apparent in the cross-shore evolution of

the spectral shape (Figs. 4 and 5). Fig. 4 displays the sea-surface elevation energy density spectra computed over a 20-min section in the nonbreaking case at (a) sensor S1 and (b) sensor S2, and Fig. 5 represents the sea-surface elevation energy density spectra computed over a 20-min section in the breaking case. The spectral peak, around 0.09 Hz (11 s) in Fig. 4 (in nonbreaking case) and around 0.07 Hz (14 s) in Fig. 5 (in breaking case), remains the dominant feature. A bulge of high-frequency energy becomes increasingly important between stations S1 and S2 in both cases. The energy at these frequencies is relatively broad-banded with no significant peak; nevertheless, unlike in Masselink (1998) for both cases, it is close to frequencies corresponding to harmonic frequencies (nF_p , where F_p indicates the spectral peak and n is a positive integer), consistent with Elgar et al. (1997) and Norheim et al. (1997). To investigate in more detail this evolution of the spectral shape, the energy in the water-surface elevation data was distributed into three components: (1) primary wave energy ($0.05 \text{ Hz} - 3/2F_p$); (2) harmonic frequency band energy ($3/2F_p - 0.4 \text{ Hz}$) and (3) total incident wave energy by adding the two preceding components. The flux of energy associated with these components was calculated from the observations (assuming shoreward progressive waves without re-

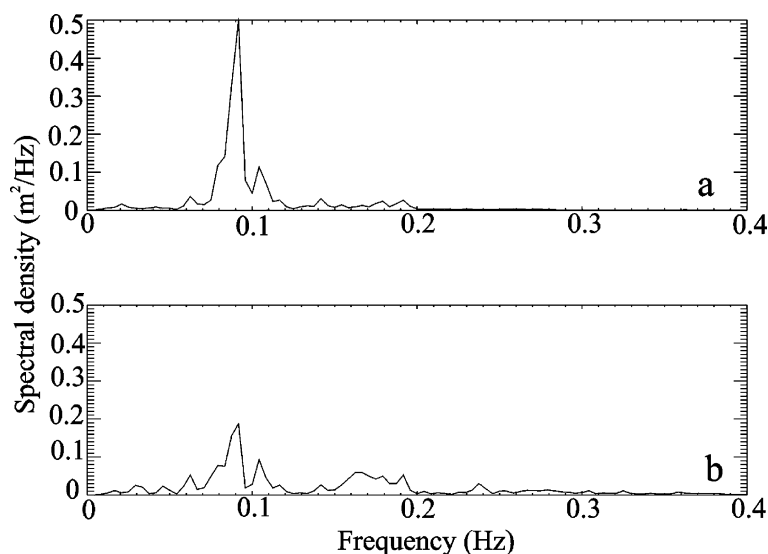


Fig. 4. Observed sea-surface elevation spectral density vs. frequency at sensors (a) S1 and (b) S2 for the nonbreaking case.

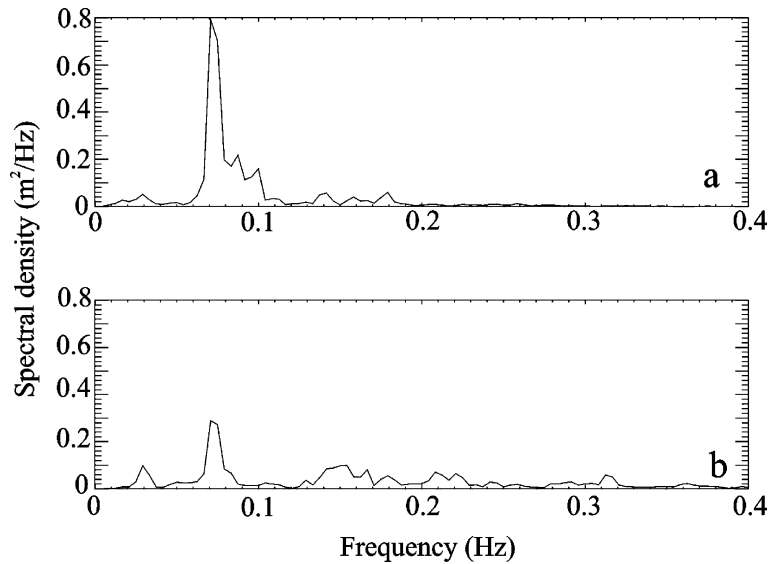


Fig. 5. Observed sea-surface elevation spectral density vs. frequency at sensors (a) S1 and (b) S2 for the breaking case.

flection) by integrating the energy flux over the frequency band:

$$EC_g = \int_{f_1}^{f_2} P(f)C_g(f)df \quad (8)$$

where C_g is the group velocity; $P(f)$ is the power spectrum associated to frequency f ; E is the total energy; and f_1 and f_2 are the cutoff frequencies of each component.

Then the flux of energy associated with these components was normalized with respect to the total incident wave energy flux measured at station S1 (Table 1). In both cases (breaking and nonbreaking), we observe an increase in the harmonic frequency band energy flux between S1 and S2 by a factor of about 3.0 in the nonbreaking case and by a factor around 2.5 in breaking case, resulting in comparable energy flux in the primary waveband and harmonic frequency band, consistent with the observations of

Elgar et al. (1997). It is apparent at this stage that the harmonic frequency band energy flux develops virtually independent of wave breaking. We also observe a decrease in the total incident wave energy flux between S1 and S2 by a factor 1.2 in nonbreaking case. This is partly due to weak nonlinear energy transfer to secondary waves with different frequency (Sénéchal et al, 2002) and also probably due to energy dissipation by weak wave crest spilling.

The 60% decrease in primary wave energy flux in breaking case is larger than in the nonbreaking case by a factor around 2.0, whereas the increase in harmonic frequency band energy is more or less the same. According to the previous results, we can deduce that wave breaking does not affect the generation of harmonic frequency band energy, consistent with Beji and Battjes (1993). Nevertheless, it does not seem to act as a secondary effect by simply rescaling the wave spectrum through overall energy dissipation as suggested by Beji and Battjes (1993). It looks as if

Table 1

Ratio of energy flux in each frequency band at sensors S1 and S2 to total incident wave energy flux at sensor S1

	Nonbreaking waves			Breaking waves		
	Total incident wave	Primary wave	Harmonic wave	Total incident wave	Primary wave	Harmonic wave
S1 sensor	1.00	0.90	0.10	1.00	0.85	0.15
S2 sensor	0.85	0.50	0.35	0.65	0.25	0.40

primary wave energy dissipates, whereas harmonic frequency band energy does not. On the other hand, maybe as already observed by Elgar et al. (1997), at frequencies near the harmonic, significant energy gain from nonlinear transfers nearly balances losses from dissipation, resulting in only a slight net energy decrease in this frequency band between the non-breaking and the breaking case. A fourth station situated in the first trough would have been useful to clearly understand the spatial evolution of each frequency band over this complex bathymetry.

4.3. Bispectral evolution

The conventional viewpoint for nonlinear coupling in waves passing over a bar is that the wave decomposition phenomenon during passage over a submerged bar settles in two stages. The first is the higher harmonic generation in shallow water where nonlinearities are strong and triad interactions are near resonant. Thus, on the seaside of the bar, the harmonics bound to the primary are amplified. In the second stage, in the trailing side of the shelf, a large amount of the phase-locked harmonic energy is transmitted as free energy because wave nonlinearity is so weak that bound waves cannot continue to exist (Ohyama and

Nadaoka, 1992). The harmonics are released. At this stage, Beji and Battjes (1993) also suggest that the dispersive tail waves are free. Use of higher-order spectral methods will allow us to determine if the energy observed in higher-frequency components (Figs. 4b and 5b) is due to nonlinear interactions and also to verify its possible release in the trough.

Fig. 6 represents the bicoherence spectrum at (a) sensor S1 and (b) sensor S2 computed over a 20-min section in a nonbreaking case. The bicoherence spectrum at the deepest sensor (Fig. 6a) indicates nonlinear coupling between modes within the power-spectral peak and modes at twice the peak's frequency. The convention is that the interactions involve f_1 , f_2 , and f_3 , where $f_3 = f_1 + f_2$. For example, $b(0.09, 0.09) = 0.35$, indicating a self-self wave interaction at $f = 0.09$ Hz coupled with energy at $f = 0.18$ Hz. Although the bispectral calculations only indicate that nonlinear coupling is occurring and not the direction of energy flow (i.e., which modes are receiving energy), the sequence of energy spectra (Fig. 4) and the evolution of the normalized energy flux (Table 1) show that energy is being received mostly by high frequencies. As the waves shoal, the excitation of phase-couple harmonics is vividly reflected in the bicoherence. In shallower water (Fig. 6b), nonlinear coupling spreads

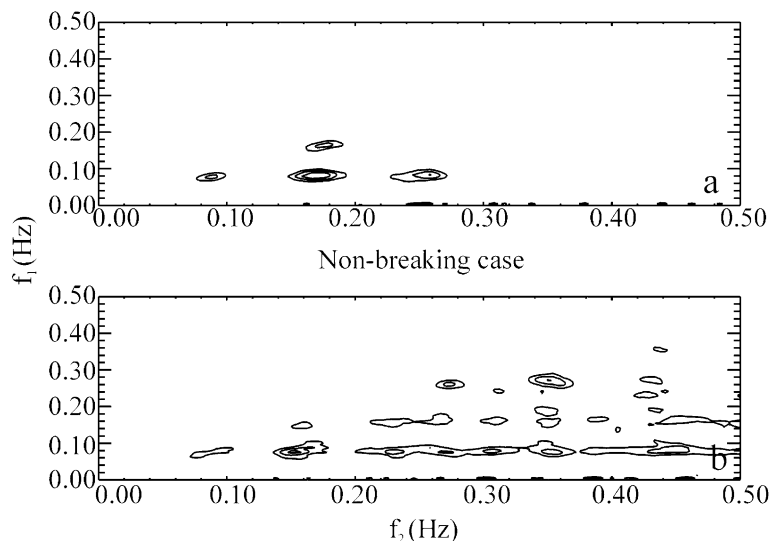


Fig. 6. Isolines of bicoherence b for sensors (a) S1 and (b) S2 in the nonbreaking case. The first isoline is 0.25 and each additional isoline is 0.10 (the 95% significance level on zero bicoherence is 0.2). At sensor (a) S1, the nonlinearity parameter defined as the ratio between significant wave height and water depth is 0.21, and it is 0.27 at sensor (b) S2.

not only to encompass interactions between the power-spectral peak and its higher harmonics, but also to encompass interactions between the harmonics themselves (Elgar and Guza, 1985; Eldeberky, 1996; Norheim et al., 1997; Becq, 1998). For example (Fig. 6b), $b(0.27, 0.27) = 0.35$; $b(0.36, 0.27) = 0.45$. Nevertheless, the interpretation of the bispectrum at sum frequencies of approximately $3F_{p1}$ is ambiguous because contributions of both secondary and tertiary forced waves may be significant. The presence of tertiary waves should be confirmed by higher-order spectral analysis such as the trispectral analysis (Elgar et al., 1995).

Another interesting result provided by the bicoherence spectrum is the weak decrease in bicoherence involving a self–self interaction at the frequency peak F_{p1} ; $b(0.09, 0.09) = 0.25$ at sensor S2, whereas $b(0.09, 0.09) = 0.35$ at sensor S1. This decrease is weaker than expected and does not support the second stage of wave decomposition phenomenon during passage over a shelf as proposed by Ohyama and Nadaoka (1992), who suggested that bound waves cannot continue to exist beyond the bar. Nevertheless, the present study features a continuously varying beach topography unlike in Ohyama and Nadaoka's (1994) study. Moreover, our results are consistent with other physical model experiments featuring varying beach

topography (Eldeberky and Battjes, 1994; Becq, 1998).

Another interesting result is obtained by computing the bicoherence spectrum over a 20-min section in a breaking case. Fig. 7 represents the bicoherence spectrum computed at (a) sensor S1 and (b) sensor S2. At sensor S1 (Fig. 7a), nonlinear couplings are very important, consistent with previous results (Fig. 6), and spread not only to encompass interactions between the power-spectral peak and its higher harmonics, but also to encompass interactions between the harmonics themselves. For example, $b(0.14, 0.14) = 0.25$ and $b(0.21, 0.21) = 0.35$. Again, the sequence of energy spectra (Fig. 5) and the evolution of the normalized energy (Table 1) confirm that energy is being received mostly by high frequencies. At sensor S2 (Fig. 7b), waves are broken. The bicoherence is near zero for all triads, suggesting that the modes are independent of each other, i.e., for random phase relationships between Fourier modes in a linear wave field. This is consistent with the results of Eldeberky (1996) and Becq (1998), who observed that bicoherence became more diffuse after breaking. At this stage, it is apparent that wave breaking substantially weakens the strength of the nonlinear couplings. Again, a fourth station situated in the first trough would have been suitable to better understand

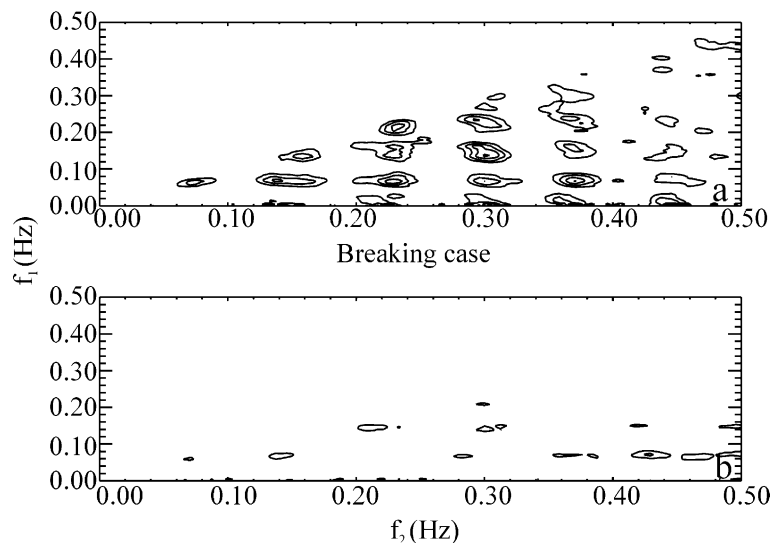


Fig. 7. Isolines of bicoherence b for sensors (a) S1 and (b) S2 in the breaking case. The first isoline is 0.25 and each additional isoline is 0.10 (the 95% significance level on zero bicoherence is 0.2). At sensor (a) S1, the nonlinearity parameter is 0.31 and it is 0.32 at sensor (b) S2.

all possible wave–wave interactions and the spatial evolution of each triad interaction.

The biphas has been computed from the bispectrum using Eq. (6) for selected frequency pairs. These pairs represent the self-interactions of the primary, denoted as (f_p, f_p) , and the interaction between the primary and the first harmonic, denoted as $(f_p, 2f_p)$. Biphases of the other interactions were not computed because no energy exists at the higher harmonics. At sensor S1, situated in the shoaling zone, the biphas of the self-interaction of the primary is near the value of $-\pi/2$, implying a wave pitched forward (nearly saw-toothed shape, Masuda and Kuo, 1981), consistent with Eldeberky (1996). Beyond the bar, at sensor S2, the biphas evolves back to a near zero value, associated with a wave of sharp peaks and broad, flat troughs, but nearly symmetrical with respect to a vertical axis (Figs. 2b and 3b), as previously observed by Eldeberky (1996). The biphas of the interaction between the primary and the first harmonic is near $-\pi/2$ at sensor S1, the same as the biphas of the self-interaction of the primary, consistent with previous works (Elgar and Guza, 1985). As the waves deshoal over the downslope side of the bar, the biphas diverges from $-\pi/2$, consistent with Eldeberky (1996).

4.4. Evolution of the wave period

The main implication of the generation of high-frequency wave energy and the consequent formation of secondary waves is a decrease in the mean wave period. Fig. 8 represents the density function of wave periods computed using the zero-downcrossing method in case of nonbreaking waves (when only a weak decrease in bicoherence is observed at station S2). We clearly distinguish a strong modification in the density function shape between sensor S1 (Fig. 8a), sensor S2 (Fig. 8b) and the ADV (Fig. 8c). The increase in the total wave number between sensor S1 (107) and sensor S2 (150) leads to a decrease in the mean period (10.9 s at sensor S1, 8.0 s at sensor S2 and 6.9 s at sensor ADV). The time domain records also indicated that the significant wave period (considered as the average period of the highest one-third of the waves of the wave train) decreased from 12.2 s at sensor S1 to 9.7 s at sensor S1 and to 8.0 s at sensor ADV, where the density function is clearly

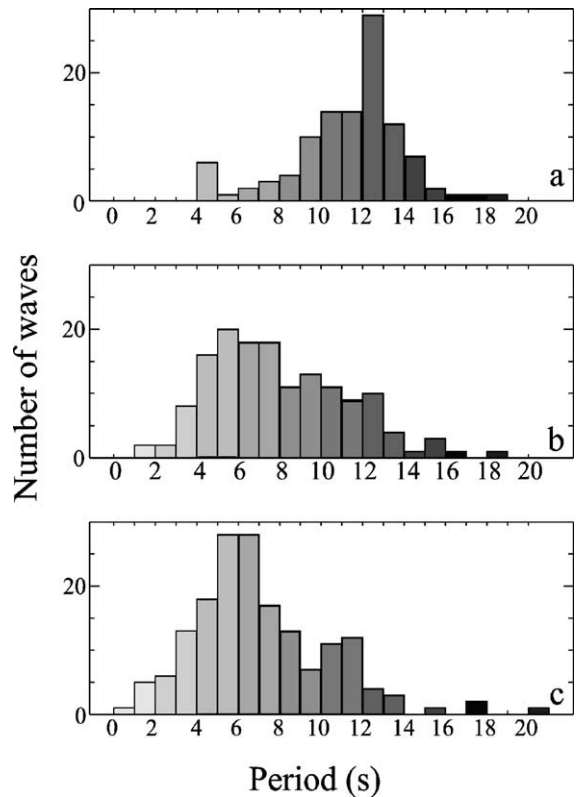


Fig. 8. Observed wave period density function at sensor (a) S1, (b) S2 and (c) ADV in the nonbreaking case.

centered around the first harmonic (6–7 s). Note that the density function shape at sensor S2 is a transitional stage between the incoming wave field (centered around the primary wave period) and the wave field at ADV (centered around the first harmonic). Further investigations, including a denser sensor line, should allow us to quantify the role of the phenomenon of harmonic shoaling, the role of primary wave dissipation (in breaking case) and the role of energy transfer in the decrease of the significant wave period.

4.5. Energy dissipation in the surf zone

The generation of secondary waves over a bar may considerably change energy dissipation in the surf zone. Indeed, the decomposition of the primary wave into shorter and smaller waves may inhibit breaking-induced energy dissipation. As underlined by Masse-

link (1998), this phenomenon has important ramifications for nearshore wave modeling. Classical, parametric wave transformation models for regular waves (Stive, 1984; Svendsen, 1984; Bonneton, 2001) or for irregular waves (Battjes and Janssen, 1978; Thornton and Guza, 1984; Hamm et al., 1993) do not account for the generation of high-frequency energy and the formation of secondary waves. Hence, in the case of nearshore bar morphology, these models will overestimate the wave period and probably underestimate the energy just beyond the bar, when a first breakpoint is present on the bar for the primary incident waves.

Fig. 9 represents the significant wave height (defined as four times the sea-surface elevation standard deviation) at total incident wave energy (0.05–0.4 Hz) vs. the depth for all the data sections (both high-tide cycles) when the stations (S2 and ADV) were in the surf zone. The result is consistent with previous field measurement observations (Wright et al., 1982; Thornton and Guza, 1982; Raubenheimer et al., 1996; Sénéchal et al., 2001), suggesting that the significant heights (H_s) of broken waves in the surf zone are depth (h)-limited. Nevertheless, one result is very eye-catching; we clearly distinguish two dissipation trends: one referring to the ADV data (cross symbols) and the other to the S2 data (star symbols).

The least-square linear fit for the ADV data (cross symbol with solid line) is:

$$H_s = 0.49h + 0.17, \quad \text{correlation coefficient} = 0.98 \quad (9)$$

The least-square linear fit for the S2 data (star symbol with solid line) is:

$$H_s = 0.35h - 0.13, \quad \text{correlation coefficient} = 0.98 \quad (10)$$

The discrepancy between the two least-square linear fit can be explained by the variation in the mean beach slope and the variation in the significant wave period. Even if the density function of wave periods appears to be similar at sensor S2 and ADV (Fig. 8b,c), it is not necessarily representative of the waves which are breaking. Indeed, visual observations indicated that not all waves were breaking, and this is confirmed by the evolution of the energy flux over the frequency band (Table 1).

To illustrate the implication of the formation of free secondary waves in the presence of low narrowband and long swell on wave energy dissipation, on the shore face (ADV data), we have applied the analytical

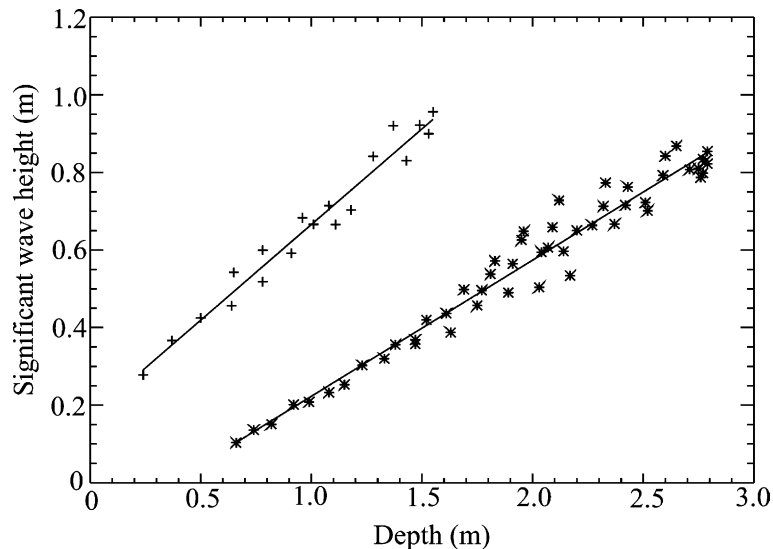


Fig. 9. Significant wave height at total incident wave energy (0.05–0.4 Hz) vs. the depth for both high-tide cycles and sensors [S2 (star symbols) and ADV (cross symbols)], when the sensors are in the surf zone, and the corresponding least-square linear fits (for both sensors, correlation coefficient is 0.98).

model of Bonneton (2001). This model has been developed for the propagation of regular waves in the inner surf zone over a constant beach slope. It resolves the steady state equation governing energy balance for waves propagating toward the shore in the inner surf zone. New estimations of the energy flux and energy dissipation for regular waves are obtained from a nonlinear wave theory, with shock conditions based on the nonlinear Saint Venant equation (SVE).

The wave height decay is given by this analytical formula:

$$\frac{H_s}{H_b} = \left[\sigma \left(\frac{h}{h_b} \right)^{-1/2} + (1 - \sigma) \left(\frac{h}{h_b} \right)^{1/4} \right]^{-1} \quad (11)$$

$$\sigma = \frac{\sqrt{3}fH_b}{\beta(g h_b)^{1/2}} \quad (12)$$

where f is the wave frequency; β is the beach slope; H_b and h_b are the height and the depth at the breakpoint, respectively.

Fig. 10 represents the model solutions and the experimental data at ADV location. The dotted–dashed line represents the solution with the offshore peak frequency, and the dotted line represents the solution with half the offshore period, which is

supposed to be the first harmonic frequency. This figure clearly shows that the solution with half the offshore peak frequency (dotted line) gives a better trend of the energy dissipation, and that classical, parametric wave transformation models, based on a conservative period, are unable to correctly predict the wave energy dissipation on the beach face in this case.

5. Discussion and conclusions

A field study was carried out for 2 days in March 2000 when long swell (11–14 s) propagated normally to a barred beach. It allowed us to investigate the phenomenon of high-frequency energy generation, observed in the power spectra of waves traveling over submerged bars (Fig. 1), and the wave decomposition phenomenon, which occurs after the bar. This paper also gives an illustration of the implications for wave dissipation energy on the beach face.

Field evidence is presented for the decomposition of incident swell into high-frequency waves during propagation over submerged bars (Figs. 2b and 3b). The bulge of high-frequency energy (Figs. 4b and 5b) is primarily ascribed to the sum interactions between pairs of waves at the primary spectral peak. Shoaling

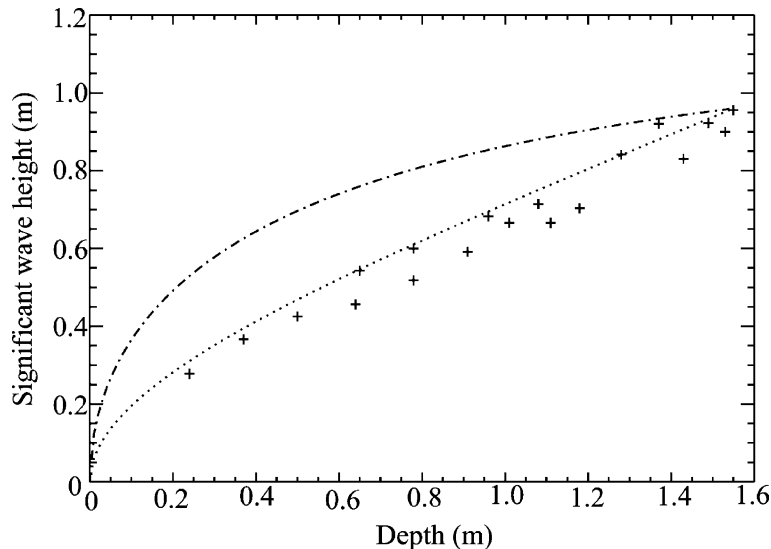


Fig. 10. Significant wave height at total incident wave energy vs. the depth for the ADV data (when the ADV is in the surf zone) and Bonneton’s model solutions: the dotted–dashed line represents the solution with the offshore peak frequency; the dotted line represents the solution with twice the offshore peak frequency (supposed to be the first harmonic frequency).

leads to phase coupling between the primary and secondary harmonic, and eventually with higher harmonics (Figs. 6a and 7a). In this region, strong non-linearity results in a profile distortion called asymmetry (Figs. 2a and 3a). Bicoherence levels observed just seaward of the wave breaking are generally high, indicating strong, nonlinear couplings (Fig. 7a). Non-linear interactions are near resonant, allowing significant net energy transfers over several wavelengths (Table 1). Wave breaking reduces the intensity of the bicoherence levels (Fig. 7b). Thus, wave breaking weakens the strength of the nonlinear couplings. On the other hand, the generation of high-frequency energy and its transfer among nearly harmonic wave components is hardly affected by wave breaking (Table 1), which seems to principally act on the primary waves (Table 1 and bispectral results). Wave breaking seems to favor the release of the harmonics. In fact, when no breaking occurs, the variation of the values of bicoherence, corresponding to nonlinear coupling between the power-spectral peak and its harmonics, is very moderate (Fig. 6b) despite the fact that significant harmonic generation takes place in the approach to the bar crest.

The release of the bound waves and the decomposition of the wavefield behind the bar cannot be completely ascribed to the increase in water depth and the weakening of wave couplings. Variations of the beach slope may play an important role in this phenomenon. In fact, strictly speaking, even in the shoaling region, free components are generated as the result of the nonhomogeneity (Eldeberky, 1996). At the top of the bar, the waves will have to adjust, from a sloping seabed to a horizontal one, and during this process, part of the bound harmonics will be released as free harmonics. At the far end of the bar and on the downward slope, more bound harmonic energy will be released due to increasing water depth (Madsen and Schäffer, 1999).

Nevertheless, a doubt exists in the interpretation of the role of the secondary bar. The wave profile characteristics are similar to those obtained when only one bar is present (Beji and Battjes, 1993; Elgar et al., 1997 and many others). This last point should be further investigated, as should the role of the beach slope.

The generation of secondary wave implies a strong modification of the wave period density function (Fig. 8); this phenomenon is of great importance for wave

dissipation in the surf zone as suggested in Figs. 9 and 10. Fig. 9 clearly shows that in this particular case, the release of the harmonics due to the presence of a bar delays the energy dissipation on the beach face.

More detailed field investigations are required to delineate more precisely the conditions under which high-frequency wave energy is generated and released as secondary waves. Particularly, a field experiment should be carried out during wind wave conditions (mean periods typically around 6–10 s) with a denser sensor line in case of single bar and multiple bar profile. The present study also shows that it is necessary to consider a large number of methods for analysis to fully (or at least, try to) understand much of the mechanisms which take place in the surf zone.

Acknowledgements

This study was performed within the framework of the Programme National d'Environnements Côtiers, project "Hydrodynamique sédimentaire en zone côtière", sponsored by CNRS/INSU. Partial support was also received from the European community under MAST contract no. MAS3-CT-0106. We would like to thank Mr. A. de Resseguier, Mr. G. Oggian and Mr. R. Butel for their contributions.

References

- Battjes, J.A., Janssen, J.P.F.M., 1978. Energy loss and set-up due to breaking in random waves. Proc. 16th Int. Conf. Coast. Eng. ASCE, vol. 1, pp. 569–587.
- Beq, F., 1998. Extension de la modélisation spectrale des états de mer vers le domaine côtier. PhD thesis, University of Toulon-Var, Toulon, France.
- Beji, S., Battjes, J.A., 1993. Experimental investigation of wave propagation over a bar. Coast. Eng. 19, 151–162.
- Bonneton, P., 2001. A note on wave propagation in the inner surf zone. C. R. Acad. Sci. Paris 329 (S II b), 27–33.
- Brossard, J., Chagdali, M., 2001. Experimental investigation of the harmonic generation by waves over a submerged plate. Coast. Eng. 42, 277–290.
- Butel, R., Dupuis, H., Bonneton, P., 2002. Spatial variability of wave conditions on the French Atlantic Coast using in situ data. To appear in Proc. ICS 2002, special issue of J. Coast. Res.
- Driscoll, A.M., Dalrymple, R.A., Grilli, S.T., 1992. Harmonic generation and transmission past a submerged rectangular obstacle. Proc. 23rd Int. Conf. Coast. Eng. ASCE, vol. 1, pp. 1142–1152.
- Eldeberky, Y., 1996. Nonlinear transformation of wave spectra in

- the nearshore zone. PhD thesis, Delft University of Technology, Delft, Netherlands.
- Eldeberber, Y., Battjes, J.A., 1994. Phase lock in waves passing over a bar. *Int. Symp.: Waves—Physical and Numerical Modeling*, Vancouver, pp. 1086–1095.
- Elgar, S., Guza, R.T., 1985. Observations of bispectra of shoaling surface gravity waves. *J. Fluid Mech.* 161, 425–448.
- Elgar, S., Herbers, T.H.C., Chandran, V., Guza, R.T., 1995. Higher-order spectral analysis of nonlinear ocean surface gravity waves. *J. Geophys. Res.* 100 (C3), 4977–4983.
- Elgar, S., Guza, R.T., Raubenheimer, B., Herbers, T.H.C., Gallagher, E.L., 1997. Spectral evolution of shoaling and breaking waves on a barred beach. *J. Geophys. Res.* 102 (C7), 15797–15805.
- Freilich, M.H., Guza, R.T., 1984. Nonlinear effects on shoaling surface gravity waves. *Philos. Trans. R. Soc. Lond.*, A 311, 1–41.
- Froidefond, J.M., Gallisaires, J.M., Prud'homme, R., 1990. Spatial variation in sinusoidal wave energy on a crescentic nearshore bar; application to the Cap Ferret coast, France. *J. Coast. Res.* 4–6, 927–942.
- Grilli, S.T., Horrilli, J., 1999. Shoaling of periodic waves over barred beaches in a fully nonlinear numerical wave tank. *J. Offshore Polar Eng.* 5, 1–18.
- Hamm, L., Madsen, Per A., Peregrine, H., 1993. Wave transformation in the nearshore zone: a review. *Coast. Eng.* 21, 5–39.
- Hasselmann, K., Munk, W., MacDonald, G., 1963. Bispectra of ocean waves. In: Rosenblatt, M. (Ed.), *Time Series Analysis*, pp. 125–139.
- Haubrich, R.A., 1965. Earth noises, 5–500 millicycles per second. *J. Geophys. Res.* 70, 1415–1427.
- Horikawa, K., Kubota, S., 1988. In: Horikawa, K. (Ed.), *Nearshore Dynamics and Coastal Processes*, Part V, pp. 386–406. Chapter 2.
- Johnson, J.W., Fuchs, R.A., Morison, J.R., 1951. The damping action of submerged breakwaters. *Trans. Am. Geophys. Union* 32 (5), 704–718.
- Kim, Y.C., Powers, E.J., 1979. Digital bispectral analysis and its application to nonlinear wave interactions. *IEEE Trans. Plasma Sci.* PS-7 (2), 120–131.
- Lafon, V., Dupuis, H., Howa, H., Froidefond, J.M., 2002. Determining ridge and runnel longshore migration rate using SPOT imagery. *Oceanol. Acta*, in press.
- Lin, P., Liu, P.L.-F., 1998. A numerical study of breaking waves in the surf zone. *J. Fluid Mech.* 359, 239–264.
- Lorin, J., Viguier, J., 1987. Hydrosedimentary conditions and present evolution of Aquitaine Coast. *Bull. Inst. Bassin Aquitaine* 41, 95–108.
- Madsen, P.A., Schäffer, H.A., 1999. A review of Boussinesq-type equations for surface gravity waves. In: Liu, P.L.F. (Ed.), *Adv. Coast. Ocean Eng.*, vol. 5, pp. 1–95.
- Masselink, G., 1998. Field investigation of wave propagation over a bar and the consequent generation of secondary waves. *Coast. Eng.* 33, 1–9.
- Masselink, G., Short, A.D., 1993. The effect of tide range on beach morphodynamics: a conceptual model. *J. Coast. Res.* 9, 785–800.
- Masuda, A., Kuo, Y.Y., 1981. A note on the imaginary part of bispectra. *Deep-Sea Res.* 28A (3), 213–222.
- McComas, C.H., Briscoe, M.G., 1980. Bispectra of internal waves. *J. Fluid Mech.* 97, 205–213.
- Norheim, C.A., Herbers, T.H., Elgar, S., 1997. Nonlinear evolution of surface wave spectra on a beach. *J. Phys. Oceanogr.* 28, 1534–1551.
- Ohyama, T., Nadaoka, K., 1992. Modeling the transformation of nonlinear waves passing over a submerged dike. *Proc. 23rd Int. Conf. Coastal Eng. ASCE*, vol. 1, pp. 526–539.
- Ohyama, T., Nadaoka, K., 1994. Transformation of nonlinear wave-train passing over a submerged shelf without breaking. *Coast. Eng.* 24, 1–22.
- Raubenheimer, B., Guza, R.T., Elgar, S., 1996. Wave transformation across the inner surf zone. *J. Geophys. Res.* 101, 25589–25597.
- Rey, V., Belrous, M., Guazzelli, E., 1992. Propagation of surface gravity waves over a rectangular submerged bar. *J. Fluid Mech.* 235, 453–479.
- Ruessink, B.G., 1998. Bound and free infragravity waves in the nearshore zone under breaking and nonbreaking conditions. *J. Geophys. Res.* 103 (C6), 12795–12805.
- Sénéchal, N., Dupuis, H., Bonneton, P., Howa, H., Pedreros, R., 2001. Observation of irregular wave transformation in the surf zone over a gently sloping sandy beach. *Oceanol. Acta* 24 (6), 545–556.
- Sénéchal, N., Bonneton, P., Dupuis, H., 2002. Infragravity wave frequency structure on a double barred beach. To appear in *Proc. ICS 2002*, special issue of *J. Coast. Res.*
- Stive, M.J.F., 1984. Energy dissipation in waves breaking on gentle slopes. *Coast. Eng.* 8, 99–127.
- Svendsen, I.A., 1984. Wave heights and set-up in a surf zone. *Coast. Eng.* 8, 303–329.
- Thornton, E.B., Guza, R.T., 1982. Energy saturation and phase speeds measured on a natural beach. *J. Geophys. Res.* 87, 9499–9508.
- Thornton, E.B., Guza, R.T., 1984. Transformation of wave height distribution. *J. Geophys. Res.* 88 (C10), 5925–5938.
- Wright, L.D., Guza, R.T., Short, A.D., 1982. Dynamics of a high-energy dissipative surf zone. *Mar. Geol.* 45, 41–62.